Jurnal Polimesin
Department of Mechanical Engineering
State Polytechnic of Lhokseumawe
http://e-jurnal.pnl.ac.id/polimesin
e-ISSN : 2549-1999 No. : 5 Month : October
p-ISSN : 1693-5462 Volume : 23 Year : 2025

Processing dates: received on 2025-09-23, reviewed on 2025-10-23, accepted on 2025-10-27 and online availability on 2025-10-31

Analysis of deformation behavior in circular and square hollow sections with wall thickness of 0.7 -1.0 mm in rotary draw bending

Syamsul Bahri Widodo[1*], Suheri Suheri[1], Faris Ahmad Mizanus Sabri[1], Zainal Arif[1], Muhammad Khairul Raziqin[2], Teuku Menazmi[2], Muhammad Safi'i[3]

[1]Department of Mechanical Engineering, University of Samudra, Langsa 24416, Indonesia

[2]Undergraduated Student of Mechanical Engineering, University of Samudra, Langsa 24416, Indonesia

[3]Department of Mechanical, University of PGRI, Semarang 50532, Indonesia

*Corresponding Author: syamsulbahri@unsam.ac.id

Abstract

Precise control of tube deformation during rotary draw bending is critical for automotive, structural, and piping applications to avoid rework and scrap. This study investigates the deformation behavior of circular (CHS) and square hollow sections (SHS), focusing on springback, ovalization, and wrinkling. ASTM A36 tubes Ø25 mm CHS and 25 × 25 mm SHS were tested with wall thicknesses of 0.7, 0.8, and 1.0 mm at bending angles of 30°, 60°, and 90° under controlled conditions. Results show that CHS consistently exhibit lower springback (≈ 2.5–5.0°) and ovalization (≈ 7–14%) than SHS, which reached up to 7.0° and 16.6%, respectively. Wrinkling occurred only in SHS, affecting all specimens bent to 90° with wall thicknesses of 0.7–0.8 mm. ANOVA identified tube geometry as the most significant factor ($F = 764$, $p < 0.001$), followed by bending angle and wall thickness, with negligible interaction effects. Unlike prior studies analyzing CHS or SHS individually, this work provides a systematic comparison under identical conditions, bridging experimental validation with practical guidelines. The findings highlight the decisive role of cross-sectional geometry in tube bending mechanics and suggest minimum thickness thresholds and compensatory tooling strategies for defect-free manufacturing.

Keywords:

Tube bending, cross-sectional geometry, springback, ovalization, wrinkling, statistical analysis

1 Introduction

Metal forming through tube bending is one of the most important and widely applied manufacturing processes in various engineering fields, ranging from construction, automotive, and transportation to shipbuilding and piping systems [1]. Bending enables tubes to be shaped into specific angles and radii without requiring joints, thus producing stronger and more economical structures with minimal connection points [2]. In practice, tube bending is often applied to both circular and square cross-sections. Both geometries are widely used, each offering distinct advantages and disadvantages with respect to structural efficiency, manufacturing feasibility, and design considerations [3-4].

In general, Circular Hollow Section (CHS) tubes possess a uniform material distribution about the neutral axis, making them more efficient in resisting loads from multiple directions, including bending, torsion, and internal pressure [5]. This symmetry explains the widespread use of CHS tubes in applications requiring isotropic strength, such as columns, piping systems, and vehicle frames [6]. However, during bending operations, CHS tubes are prone to specific deformation phenomena. One of the most common is ovalization, where the circular cross-section becomes elliptical due to the combined effect of bending moment and radial stresses [7]. Ovalization becomes more pronounced with increasing bending angle or decreasing bending radius [8]. In addition, CHS tubes often exhibit springback, where the bent angle partially recovers after the external load is released, creating challenges for dimensional accuracy in manufacturing [9-10].

By contrast, Square Hollow Section (SHS) tubes display different deformation behavior. The flat sides and sharp corners of SHS tubes result in a non-uniform stress distribution during bending[11-12]. The inner bend region is prone to stress concentration and wrinkling, while the outer bend region is susceptible to excessive stretching and wall thinning [13]. Furthermore, SHS tubes are more likely to experience cross-sectional distortion, including dimensional changes in the flat sides and deformation of the corners, compared to CHS tubes [14]. Nevertheless, SHS tubes offer advantages in terms of directional stability, particularly in planar frame applications and structural assemblies [15-16].

Numerous studies have sought to explain deformation phenomena in tube bending. Studied thin-walled SHS steel tubes (25×25×2 mm, S235JR) and reported that cross-sectional deformation became significant when curvature exceeded 2.0 m^{-1}, while local wall collapse occurred at 6.0 m^{-1}. For CHS tubes, parameters such as outer diameter, wall thickness, and span length were found to influence bending strength and post-failure capacity, with increasing wall thickness delaying ovalization and improving load-carrying capacity. These studies highlight the critical role of cross-sectional geometry in governing tube deformation during bending [17-18].

Recent developments in tube-bending research have focused on optimizing deformation control through advanced tooling and digital monitoring. Wang et al. (2025) introduced a diameter-adjustable mandrel that significantly improves bending accuracy for thin-wall tubes [6]. Similarly, Li et al. (2025) developed a digital-twin-based deformation monitoring system for real-time defect prediction during rotary draw bending [13]. Studies by Sun et al. (2024) and Mohammed & Cashell (2021) further explored the influence of temperature control and cross-sectional geometry on local instability during bending [7]. Despite these advances, a direct comparative analysis between CHS and SHS geometries under identical experimental parameters remains limited. Therefore, this study aims to bridge this knowledge gap by systematically quantifying springback, ovalization, and wrinkling in both tube types. Key questions arise regarding: (i) how differences in cross-sectional geometry affect springback, ovalization, and defect formation; (ii) the influence of wall thickness and bending angle on bending moment capacity and structural stability; and (iii) whether distinct failure patterns, such as intrados wrinkling or extrados thinning, can be clearly distinguished between the two geometries. Addressing these issues is essential not only for advancing academic understanding but also for providing practical guidelines to optimize tube bending operations in manufacturing industries.

2 Methodology

This study employed a systematic experimental approach to investigate the deformation behavior of circular (CHS) and square (SHS) tubes under controlled bending operations. The methodology was designed to ensure reproducibility, statistical validity, and direct relevance to manufacturing practices.

This study experimentally investigates the deformation behavior of SHS and CHS during bending. Tubes with wall thicknesses of 0.7, 0.8, and 1.0 mm were bent at angles of 30°, 60°, and 90° using

a bending machine operating at a constant speed of 30 mm/min. The analysis focuses on three key deformation phenomena: springback, ovalization, and wrinkling. Results highlight how wall thickness and bending angle influence dimensional accuracy and structural integrity. The findings provide insights for optimizing bending processes and minimizing defects in manufacturing applications of tubular components (Fig. 1).

Fig. 1. Experimental schematic diagram

2.1 Experimental device

The bending tests were conducted using a rotary draw bending machine (Fig. 2), which provides controlled bending angles and ensures repeatability. The bending radius, speed, and specimen length were kept constant throughout the experiments to serve as control variables. Bending angles of 30°, 60°, and 90° were selected to represent light, medium, and severe bending conditions.

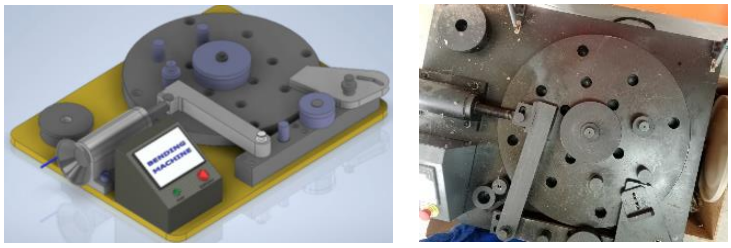

Fig. 2. Bending machine

The rotary draw bending machine (Fig. 2) was equipped with a fixed bending radius of 75 mm (corresponding to 3D, where D = 25 mm). The setup used a standard rotary-draw configuration without a mandrel or pressure die to isolate the geometric effects of tube shape. The clamping die and bending die were made of hardened steel, with groove profiles matching the outer diameter or side length of each specimen.

The experimental specimens consisted of ASTM A36 tubes: CHS with an outer diameter of Ø25 mm and SHS with a nominal cross-section of 25 × 25 mm; each geometry was tested with wall thicknesses of 0.7, 0.8, and 1.0 mm. A material widely used in construction due to its good balance of strength and ductility. Two geometries were investigated:

- CHS : 25 mm outer diameter, 500 mm length.
- SHS : 25 × 25 mm cross-section, 500 mm length.

2.2 Experimental design and measurements

The bending angle was measured using a digital angle gauge, calibrated against a certified reference block before each test. The tool alignment and bending radius were verified using a coordinate measuring arm (accuracy ±0.02 mm). Calibration of the measurement system was performed before testing by comparing the recorded bending angle of a rigid reference specimen to the programmed machine setting; deviations were within ±0.1°. All instruments complied with ISO 2768 standard tolerances.

A factorial experimental design was adopted, considering three main factors: Shape (CHS vs. SHS), Bending Angle (30°, 60°, and 90°), and Wall Thickness (0.7, 0.8, and 1.0 mm). Each condition was repeated three times to ensure statistical reliability, resulting in a total of 54 experimental runs.

The combination of these parameters yielded 18 testing conditions, which served as the basis for this comparative study. The variation in wall thickness was selected to evaluate the extent to which tube wall stiffness influences deformation behavior, as thin-walled tubes are generally more prone to shape distortion compared to thick-walled tubes. Meanwhile, the variation in bending angle provided insight into deformation levels under light, moderate, and severe bending conditions. Through the experiments in Table 1, a more comprehensive understanding of the differences in deformation behavior between square and circular tubes is expected, while simultaneously analyzing the influence of wall thickness and bending angle on the quality of the bending.

Wrinkling on the intrados surface was quantified using a digital optical profilometer (Keyence VR-5000, resolution 1 μm) to measure the amplitude of surface undulations over a 30 mm gauge length. A specimen was classified as wrinkled if the maximum wrinkle amplitude (Amax) exceeded 0.15 mm or if the ratio Amax/t > 0.2, where t is the wall thickness. Measurements were performed at 5× magnification, and each reading was averaged over three locations along the bend region. Specimens below this threshold were considered wrinkle-free. The quantitative results were subsequently cross-checked with visual inspection to confirm the reliability of the optical measurements.

Table 1. Experimental parameters

Parameter	Levels/values	Notes
Tube shape	CHS (Ø25 mm), SHS (25 × 25 mm)	ASTM A36 steel
Wall thickness	0.7, 0.8, 1.0 mm	Independent variable
Bending angle	30°, 60°, 90°	Independent variable
Bending speed	30 mm/min	Constant
Specimen length	500 mm	Constant
Bend radius	Fixed (machine standard)	Constant

The mechanical properties of ASTM A36 steel used in this study are summarized in Table 2. Tensile tests were performed to determine the yield and ultimate tensile strengths as well as Young's modulus. At the same Time, the Poisson's ratio and elongation values were adopted from standard references for ASTM A36 steel. These properties ensure adequate ductility and stiffness suitable for bending operations.

Table 2. Mechanical properties of ASTM A36 steel used in the experiments

Property	Symbol	Value	Unit
Yield strength	σ_y	≈ 250	MPa
Ultimate tensile strength	σ_u	400-550	MPa
Young's modulus	E	≈ 200	GPa
Poisson's ratio	ν	0.26-0.30	-

The deformation behavior of the tubes was evaluated using three response variables:

1. Springback (Δθ)

Measured as the difference between the target bending angle θ_{target} and the actual angle after unloading θ_{actual}. Springback (Δθ) can be obtained by Eq. (1).

$$\Delta\theta = \theta_{target} - \theta_{actual} \quad (1)$$

2. Ovalization (%)

For CHS specimens, ovalization was determined using the maximum (D_{max}) and minimum (D_{min}) diameters after bending. Ovalization can be obtained by Eq. (2).

$$Ovalization\ (\%) = \frac{D_{max} - D_{min}}{D_0} \times 100 \quad (2)$$

where D_{max} is the initial diameter for SHS specimens, distortion was assessed by changes in length (S) and corner angle (θ) compared to the undeformed state.

3. Wrinkling (binary)

Wrinkling at the intrados surface was inspected visually and recorded as Yes/No.

2.3 Specimen preparation

Test preparation is carried out in several stages: specimen preparation, bending machine setup, and bending results data analysis.

2.3.1 Specimen preparation

The specimen preparation stage involved determining the types of specimens and the material properties required for the experimental work. Two types of specimens were used: CHS and SHS tubes, both commonly used in structural components in the construction and manufacturing industries. Each specimen was cut to 500 mm in length using a cutting saw. The initial dimensions, length, diameter, and wall thickness were measured and recorded before the bending tests. Fig. 3 shows the prepared CHS and SHS specimens.

SHS (0.7, 0.8, 1.0 mm Wall Thickness) CHS (0.7, 0.8, 1.0 mm Wall Thickness)

Fig. 3. CHS and SHS specimens

2.3.2 Bending machine setup

The setup of the bending machine began with an inspection of all components to be used during testing. The bending machine components were inspected to ensure proper condition and compliance with standard operating procedures. The next step was to verify that the machine operation followed the standard operating procedures (SOP). The setup process was also adjusted according to the predefined experimental parameters.

2.3.3 Bending result data analysis

The experimental data were analyzed using both descriptive statistics (mean and standard deviation) and inferential statistics. Analysis of variance (ANOVA) was performed to determine the significance of primary factors and interactions on spring back. Defect occurrence rates were calculated using frequency analysis. Graphs and interaction plots were generated to visualize the effects of variables on deformation behavior. The methodology ensures that the results not only provide insights into material deformation but also deliver practical implications for manufacturing optimization.

3 Results and discussion

3.1 Descriptive analysis

Table 3 summarizes the descriptive statistics of the experimental results, including the mean and standard deviation of springback and ovalization, as well as the occurrence of wrinkling defects (Eqs. 1 and 2). The results clearly indicate that tube shape, bending angle, and wall thickness strongly influence the deformation behavior. HS springback ≈ 5.0°, SHS ≈ 7.0°; CHS ovalization ≈ 14%, SHS ≈ 16.6%. Fig. 4. Bending results for (a) 30°, (b) 60°, and (c) 90° angles showing CHS (Ø25 mm) and SHS (25 × 25 mm) specimens, each tested with wall thicknesses of 0.7, 0.8, and 1.0 mm.

Circular tubes (CHS) exhibit lower springback compared to square tubes (SHS) across all bending angles. For example, at a bending angle of 90° with 1 mm thickness, the springback of SHS reached an average of 7°, while CHS remained at approximately 5°. This demonstrates that the cross-section geometry significantly affects stress distribution during bending, with SHS being more prone to elastic recovery after unloading.

Table 3. Descriptive statistics of bending results for CHS and SHS tubes (mean ± SD, Defect %)

Shape	Bending angle (deg)	Wall yhickness (mm)	Spring back (Mean ± SD)	Ovalization (Mean ± SD)	Defect (%)
CHS	30	0.7	2.50 ± 0.15	7.00 ± 0.56	0
CHS	30	0.8	2.67 ± 0.29	8.14 ± 0.33	0
CHS	30	1	2.73 ± 0.25	7.69 ± 0.49	0
CHS	60	0.7	3.43 ± 0.35	11.93 ± 0.87	0
CHS	60	0.8	3.37 ± 0.15	11.03 ± 0.17	0
CHS	60	1	4.03 ± 0.25	9.99 ± 0.35	0
CHS	90	0.7	4.37 ± 0.32	14.75 ± 0.6	0
CHS	90	0.8	4.43 ± 0.21	14.00 ± 0.47	0
CHS	90	1	5.0 ± 0.17	14.00 ± 0.62	0
SHS	30	0.7	4.47 ± 0.25	11.32 ± 0.57	0
SHS	30	0.8	4.53 ± 0.25	10.0 ± 0.64	0
SHS	30	1	5.03 ± 0.12	9.77 ± 0.36	0
SHS	60	0.7	5.2 ± 0.44	14.06 ± 0.27	100
SHS	60	0.8	5.7 ± 0.26	12.64 ± 0.59	100
SHS	60	1	6.0 ± 0.26	12.85 ± 0.47	0
SHS	90	0.7	6.37 ± 0.12	16.62 ± 0.94	100
SHS	90	0.8	6.33 ± 0.47	15.98 ± 0.16	100
SHS	90	1	7.00 ± 0.15	16.53 ± 0.66	100

*Wrinkling classification based on Amax > 0.15 mm or Amax/t > 0.2 (measured by optical profilometer

Similarly, ovalization increases as the bending angle becomes larger and the wall thickness decreases. Thin-walled tubes (0.7 mm) showed ovalization levels exceeding 10%, particularly in SHS specimens. CHS tubes maintained lower ovalization (7–14%), while SHS reached up to 16%, confirming that wall thickness is a critical parameter for maintaining dimensional accuracy during bending operations. Defect occurrence analysis also revealed that wrinkling appeared most frequently in SHS tubes bent at 90°, with a defect rate of up to 100% of the samples (Fig. 4). This

phenomenon is associated with local instability at the intrados wall under severe bending conditions.

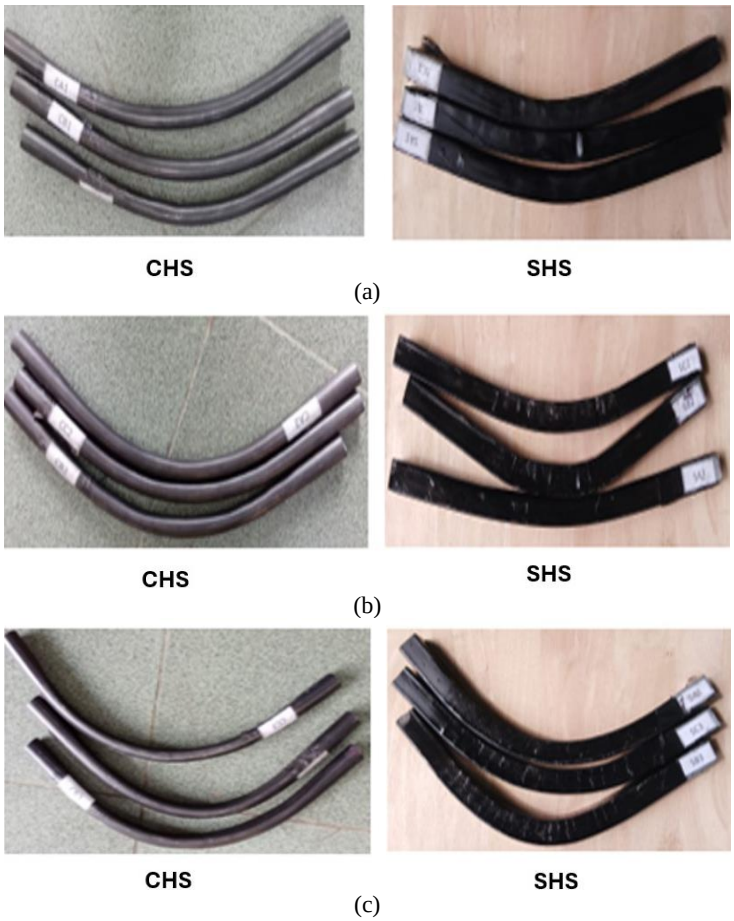

Fig. 4. Bending results: (a) 30º, (b) 60º, and (c) 90º bending angle

3.2 ANOVA analysis

The Analysis of Variance (ANOVA) results confirm the observed trends. Springback and ovalization were significantly influenced by Shape, Bending Angle, and Wall Thickness ($p < 0.05$) in Table 4. Among these, Shape exerted the most potent effect, indicating that the distinction between CHS and SHS is the most critical factor. Bending Angle was the next most influential, followed by Wall Thickness. Interaction effects were not statistically significant, suggesting that these parameters operate independently.

Table 4. ANOVA results for springback

Factor	Sum Sq	Df	F	p-value
Shape	54.60	1	763.86	<0.001
Bending angle	33.45	2	233.96	<0.001
Wall thickness	3.34	2	23.35	<0.001
Interactions	n.s.	-	-	n.s.

*Shapiro–Wilk and Levene tests confirmed normality and homogeneity ($p > 0.05$) for all datasets

Before performing ANOVA, data normality was verified using the Shapiro–Wilk test, and homogeneity of variance was assessed using the Levene test at a 95% confidence level. The results confirmed that all datasets satisfied the assumptions of normality ($p > 0.05$) and homogeneity of variances ($p > 0.05$). Residual plots for both springback and ovalization exhibited random dispersion around zero, indicating no systematic deviation from the model assumptions. Consequently, no data transformation or nonparametric alternative was required. All analyses were performed using Minitab® 21.1 software.

The ANOVA results highlight several key insights. First, the tube geometry (CHS vs SHS) is the dominant factor controlling both springback and ovalization, which aligns with the descriptive analysis. CHS, due to its cylindrical symmetry, distributes stresses uniformly, whereas SHS suffers from stress concentrations at flat sides and corners, explaining its poorer bending performance. Second, bending angle strongly affects deformation: larger angles amplify elastic recovery and dimensional distortion. Finally, wall thickness contributes to structural stability, with thinner tubes being more prone to ovalization and defects (Table 5). These statistical findings reinforce the practical guidelines for manufacturing optimization, suggesting that CHS tubes and thicker walls should be preferred when high-dimensional accuracy and defect-free results are required.

Table 5. ANOVA results for ovalization

Factor	Sum Sq	Df	F	p-value
Shape	62.38	1	208.25	<0.001
Bending Angle	298.75	2	498.65	<0.001
Wall Thickness	17.62	2	29.42	<0.001
Interactions	n.s.	-	-	n.s.

*Shapiro–Wilk and Levene tests confirmed normality and homogeneity ($p > 0.05$) for all datasets

3.3 Discussion

The present findings clearly demonstrate that tube geometry, bending angle, and wall thickness each play decisive roles in governing deformation behavior during rotary draw bending. Among these variables, tube shape emerged as the most influential factor, as confirmed both by descriptive statistics and ANOVA. CHS tubes consistently exhibited superior bending performance compared to SHS tubes. Their symmetric cross-section enabled more uniform stress redistribution, resulting in lower springback, reduced ovalization, and no wrinkling under all tested conditions.

The verified results confirm that ovalization decreases with increasing wall thickness. Specifically, tubes with t = 0.7 mm experienced the highest ovalization levels (up to 16.6% for SHS and 14.7% for CHS), while t = 1.0 mm specimens showed substantially lower distortion (<10%). The reduced flexural rigidity and greater susceptibility to cross-sectional collapse in thin-walled tubes can explain this behavior. During bending, the inner wall experiences compressive stress while the outer wall is subjected to tensile stress; in thinner sections, the local plastic deformation at these zones cannot be evenly redistributed, resulting in more pronounced cross-sectional flattening. Conversely, thicker walls provide greater resistance to radial compression, mitigating ovalization.

The contrast between CHS and SHS is most evident (Fig. 5), which illustrates springback as a function of wall thickness. CHS specimens consistently recorded lower springback across all bending angles and thicknesses, whereas SHS specimens exhibited markedly higher values, especially at 90°. This trend highlights the geometric disadvantage of SHS tubes, where flat surfaces and corners promote elastic recovery after unloading [19].

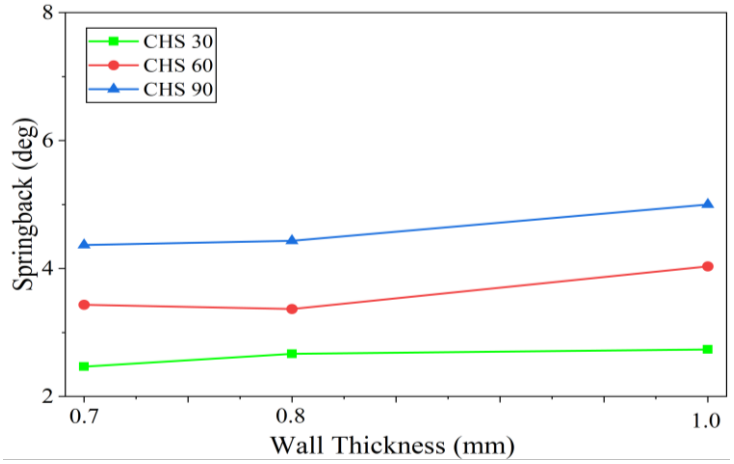

Fig. 5. Springback vs wall thickness for CHS

Fig. 5 shows the effect of wall thickness on springback in CHS tubes bent at 30°, 60°, and 90°. Springback decreases gradually with increasing wall thickness for all bending angles. At 30°, values range from approximately 2.5° to 2.8°, while at 60° they increase moderately to about 3.3°–4.0°, and at 90° they reach

around 4.4°–5.0°. The overall trend indicates that thinner walls (0.7 mm) exhibit greater springback due to lower flexural rigidity and higher elastic recovery, whereas thicker walls (1.0 mm) show smaller angular deviation after unloading. Furthermore, larger bending angles lead to greater springback due to greater bending-induced elastic energy. These observations show that both wall thickness and bending angle significantly affect the dimensional accuracy of CHS bending.

Fig. 6, where ovalization increased with higher bending angles and thinner walls. Once again, CHS maintained more moderate levels of distortion, typically 7%-14%, while SHS reached 16%. The vulnerability of SHS becomes particularly evident in thin-walled conditions (0.7 mm), where dimensional collapse is more pronounced. This reinforces the critical role of wall thickness in maintaining cross-sectional integrity [20].

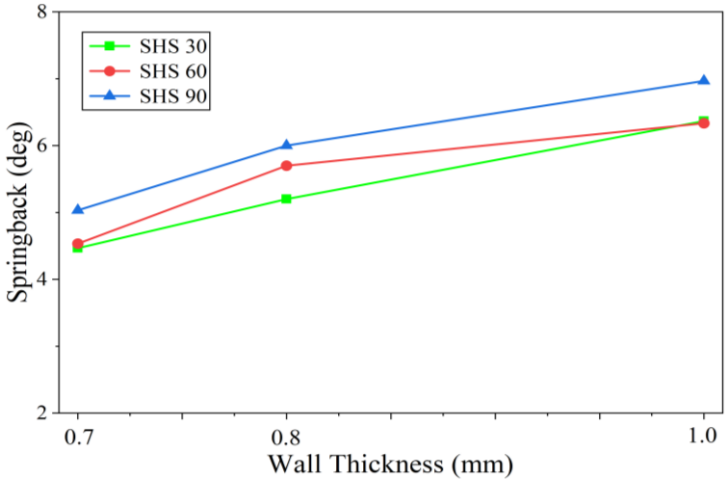

Fig. 6. Springback vs wall thickness for SHS

Fig. 7 The effect of wall thickness on ovalization in CHS tubes bent at 30°, 60°, and 90°. Ovalization increases steadily with wall thickness, showing higher distortion at 1.0 mm compared to 0.7 mm. Interestingly, tubes bent at 30° exhibit the highest ovalization (≈9–15%), followed by 60° and 90°. This indicates that at smaller bending angles, cross-sectional distortion is more pronounced, while larger angles allow for better stress redistribution and reduced ovalization. Overall, both wall thickness and bending angle significantly influence ovalization, emphasizing the need to control these parameters to ensure dimensional stability in tube bending processes.

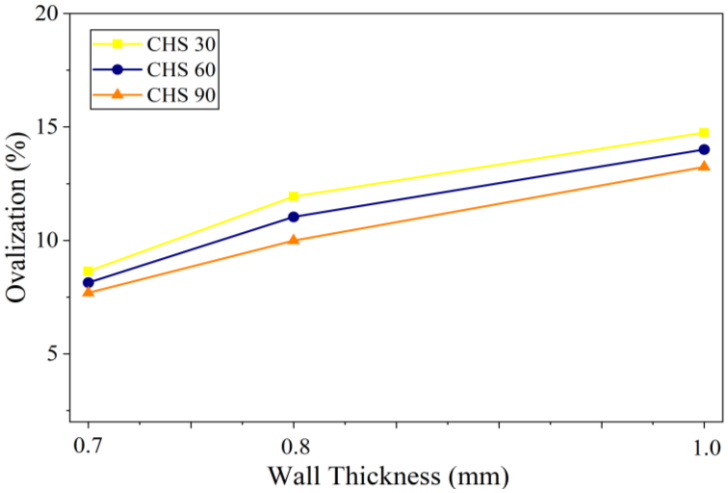

Fig. 7. Ovalization vs wall thickness for CHS

Fig. 8 The effect of wall thickness on ovalization in SHS (Square Hollow Section) tubes bent at 30°, 60°, and 90°. Ovalization values remain relatively low compared to CHS, ranging from about 4% to 7%. As wall thickness increases, ovalization shows a slight upward trend for all bending angles. Among them, the 90° bend exhibits the highest ovalization, followed by 60° and 30°. This indicates that SHS tubes are more resistant to cross-sectional distortion than CHS due to their geometric stiffness. However, higher bending angles and thinner walls still contribute to increased deformation.

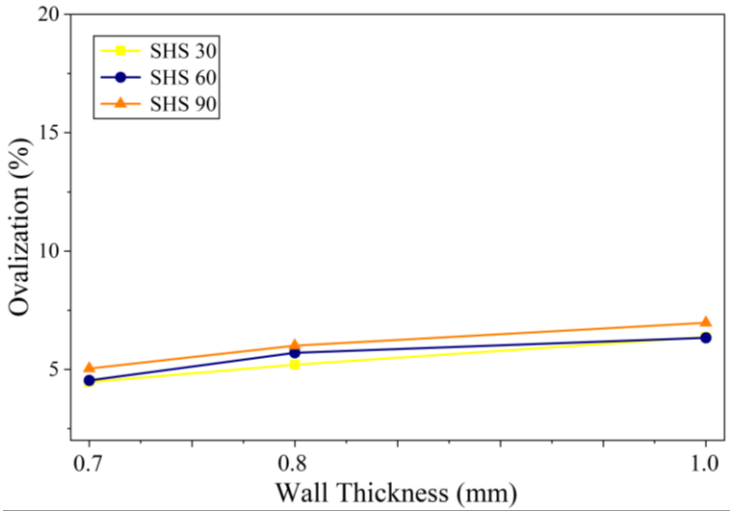

Fig. 8. Ovalization vs wall thickness for SHS

The most striking contrast is captured in Fig. 9, which illustrates wrinkling defect occurrence. While CHS remained completely free from wrinkling across all bending conditions, SHS displayed severe instability at the intrados. At 60° and 90° with thin walls, defect rates for SHS reached 100%. These results underline the structural limitations of SHS geometry, where compressive stresses on flat surfaces cannot be accommodated without local buckling [21].

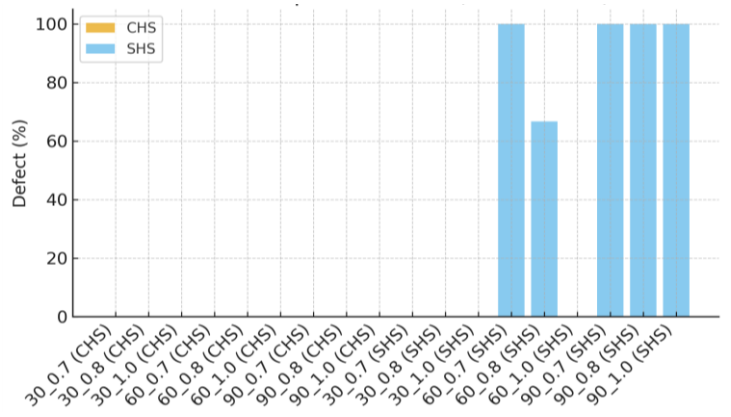

Fig. 9. Wrinkling defect occurrence (%)

The statistical analysis reinforces these experimental observations. ANOVA identified shape as the dominant factor influencing both springback and ovalization, followed by bending angle and wall thickness. The absence of significant interaction effects indicates that each factor governs deformation behavior independently, simplifying optimization strategies in manufacturing.

Taken together, the combination of Fig. 5 to Fig. 9 with the statistical analysis provides a coherent explanation of the observed trends. CHS tubes are inherently more stable and reliable for applications requiring dimensional precision, whereas SHS tubes demand additional process control. To mitigate the risks associated with SHS bending, strategies such as over-bending compensation, increased wall thickness, or the use of mandrels and specialized dies become necessary. These findings not only align with theoretical expectations of plastic deformation mechanics but also highlight the practical importance of selecting the appropriate geometry in tube bending operations.

3.4 Practical implications

The comparative analysis between CHS and SHS tubes has important implications for industrial tube-bending practices. The consistent superiority of CHS, as demonstrated in Fig. 5 and Fig. 6, indicates that circular sections should be prioritized in applications where dimensional accuracy and structural stability are critical. The

lower springback and reduced ovalization of CHS translate directly into fewer corrective measures and more predictable bending outcomes.

For SHS tubes, however, the challenges are more evident. Their higher springback values require greater overbending compensation to achieve the desired final geometry. This requirement is particularly pronounced at severe bending angles, as reflected in Fig. 5, where SHS consistently deviates more from target angles than CHS. Similarly, the greater ovalization observed in SHS Fig. 6 suggests that stricter tolerances must be applied in design and process planning when square sections are used.

The defect occurrence illustrated in Fig. 7 provides the strongest warning for SHS applications. Wrinkling rates of up to 100% in thin-walled SHS at 60° and 90° bends highlight the necessity of additional tooling, such as mandrels or specifically designed dies, to stabilize the tube wall. Without such measures, the risk of scrap production becomes unacceptable for industrial-scale manufacturing.

Finally, wall thickness emerges as a practical design parameter that can mitigate many of these issues. Maintaining a minimum wall thickness of 0.8 mm substantially reduces ovalization and defect rates, particularly in SHS tubes. Although this recommendation may lead to slightly higher material costs, it ensures higher-quality bends and reduces rework or wastage, thereby improving overall manufacturing efficiency.

3.4.1 Summary of findings

The results of this study provide a comprehensive understanding of how tube geometry, bending angle, and wall thickness affect deformation behavior during rotary draw bending. Across all tested conditions, CHS consistently outperformed SHS, exhibiting lower springback, reduced ovalization, and complete resistance to wrinkling. These advantages are clearly illustrated in Fig. 5 and Fig. 6, where CHS demonstrates more stable responses to variations in wall thickness in Fig. 7, which confirms the absence of wrinkling in CHS.

SHS tubes showed significant weaknesses, with higher springback, greater ovalization, and a strong tendency to develop wrinkling, especially at severe bending angles and reduced wall thicknesses. These findings emphasize the geometric disadvantages of SHS, where stress concentrations at flat surfaces and corners promote elastic recovery, cross-sectional distortion, and local buckling.

The statistical analysis (ANOVA) reinforced these experimental observations, identifying shape as the dominant factor, followed by bending angle and wall thickness, with no significant interaction effects. This independence means that each factor can be addressed separately in process optimization, providing a clear path for industrial improvements.

The findings highlight a fundamental conclusion: CHS tubes are inherently more reliable and dimensionally stable for bending applications, while SHS tubes require careful process adjustments, thicker walls, or specialized tooling to achieve comparable quality. This knowledge provides both theoretical validation and practical guidance for industries where precision tube bending is essential.

4 Conclusions

This study confirmed that tube geometry, bending angle, and wall thickness strongly affect deformation behaviour during rotary draw bending. Among these factors, tube shape was the most influential, with CHS exhibiting lower springback (2.5–5.0°) and ovalization (7–14%) and showing no observable wrinkling within the current experimental conditions. These findings are valid within the tested wall-thickness range (0.7–1.0 mm) and bending radius (3D); minor wrinkling could occur under more severe conditions or thinner sections. Based on the experimental results, a minimum wall thickness of 0.8 mm is recommended for SHS tubes to prevent excessive ovalization and wrinkling, especially for bending angles > 60° when no mandrel is used. For severe bending (90°), an over-bending compensation of 1.5°–2.0° can offset the higher springback in SHS compared to CHS. Additionally, the use of mandrel support or thicker walls is advised to improve dimensional stability. These findings directly link the results to practical tube-bending applications, providing actionable guidance for defect-free manufacturing. From a practical standpoint, the results suggest that CHS should be prioritized in applications requiring high-dimensional accuracy and defect-free performance. When SHS is required, compensatory measures such as overbending, thicker walls, or mandrels and specialized dies become essential to ensure acceptable product quality.

Acknowledgments

The author would like to express sincere appreciation and gratitude to the Rector of Universitas Samudra for the opportunity and support provided through the Lecturer Research Scheme funded by DIPA UNSAM in 2025, with LPPM contract number 77/UN54.6/PT.01.03/2025.

References

[1] Zili Wang, Le Wang, Shuyou Zhang, Xiaojian Liu, Yongzhe Xiang, Yaochen Lin, Jianrong Tan, "Analytical springback modelling for thermal-mechanical bending of TA18 tube under non-isothermal loading," *Appl Math Model*, vol. 143, Jul. 2025, doi: 10.1016/j.apm.2025.115964.

[2] Manahel Shahath Khalaf, Amer M. Ibrahim, Hadee Mohammed Najm, Mohanad Muayad Sabri Sabri, Samadhan Morkhade, Ashish Agarwal, Mohammed A. Alamir6and Ibrahim M. Alarifi, "Experimental Analysis of Steel Circular Hollow Section under Bending Loads: Comprehensive Study of Mechanical Performance," *Materials*, vol. 15, no. 12, Jun. 2022, doi: 10.3390/ma15124350.

[3] L. M. Alves, R. M. Afonso, and P. A. F. Martins, "A new deformation assisted joining process for connecting tubes to stronger tubesheets," *Thin-Walled Structures*, vol. 173, Apr. 2022, doi: 10.1016/j.tws.2022.108975.

[4] S. Groth, P. Frohn, and B. Engel, "Product planning system for manufacture-oriented modeling of freeform bend tubes produced by three-roll-push-bending," Elsevier B.V., 2019, pp. 10–18. doi: 10.1016/j.promfg.2019.06.107.

[5] Y. Chen, R. Feng, and W. Gong, "Flexural behavior of concrete-filled aluminum alloy circular hollow section tubes," *Constr Build Mater*, vol. 165, pp. 173–186, Mar. 2018, doi: 10.1016/j.conbuildmat.2017.12.104.

[6] Z. Wang, J. Li, X. Liu, S. Zhang, Y. Lin, and J. Tan, "Diameter-adjustable mandrel for thin-wall tube bending and its domain knowledge-integrated optimization design framework," *Eng Appl Artif Intell*, vol. 139, Jan. 2025, doi: 10.1016/j.engappai.2024.109634.

[7] H. Sun, H. Li, H. Yang, J. Ma, X. Hao, and M. W. Fu, "Breaking through the bending limit of Al-alloy tubes by cryogenic effect controlled mechanical properties and friction behaviours," *Int J Mach Tools Manuf*, vol. 195, Feb. 2024, doi: 10.1016/j.ijmachtools.2023.104111.

[8] Z. Tian, Y. Liu, L. Jiang, W. Zhu, and Y. Ma, "A review on application of composite truss bridges composed of hollow structural section members," Feb. 01, 2019, *Chang'an University*. doi: 10.1016/j.jtte.2018.12.001.

[9] Zili Wang, Jie Li, Yujun Yuan, Shuyou Zhang, Weifei Hu, Jun Ma, Jianrong Tan, "Digital-twin-enabled online wrinkling monitoring of metal tube bending manufacturing: A multi-fidelity approach using forward-convolution-GAN," Appl Soft Comput, vol. 171, Mar. 2025, doi: 10.1016/j.asoc.2024.112684.

[10] A. Borković, B. Marussig, and G. Radenković, "Geometrically exact static isogeometric analysis of arbitrarily curved plane Bernoulli–Euler beam," *Thin-Walled Structures*, vol. 170, Jan. 2022, doi: 10.1016/j.tws.2021.108539.

[11] Nuno Silvestre, António P.C. Duarte, João P. Martins, Luís Simões da Silva, "GBT Buckling Analysis of Cylindrical Panels Under Compression", Elsevier, vol. 17, pp. 34-42, Feb. 2019, doi.org/10.1016/j.istruc.2018.12.007

[12] B. Li, "Human nature, the means-ends relationship, and alienation: Themes for potential East-West collaboration," *Technol Soc*, vol. 43, pp. 60–64, Nov. 2015, doi: 10.1016/j.techsoc.2015.03.005.

[13] Jie Li, Zili Wang, Shuyou Zhang, Jingjing Ji, Yongzhe Xiang, Dantao Wang, Jianrong Tan, "Digital-Twin virtual model real-time construction via spatio-temporal cascade reconstruction for full-field plastic deformation monitoring in metal tube bending manufacturing," Robot Comput Integr Manuf, vol. 91, Feb. 2025, doi: 10.1016/j.rcim.2024.102860.

[14] Zili Wang, Yonglin Tao, Shuyou Zhang, Xiaojian Liu, Yaochen Lin, Liangyou Li, Jianrong Tan, Zheyi Li, "Spatial spiral tube multi-roller bending: Accurate axial prediction utilizing AWPSO-FECAM-LSTM framework," Expert Syst Appl, vol. 296, Jan. 2026, doi: 10.1016/j.eswa.2025.128960.

[15] P. Albertelli and M. Strano, "Tube bending machine modelling for assessing the energy savings of electric drives technology," *J Clean Prod*, vol. 154, pp. 83–93, Jun. 2017, doi: 10.1016/j.jclepro.2017.03.212.

[16] C. Wang, G. Yu, W. Wang, and J. Zhao, "Deflection detection and curve fitting in three-roll continuous straightening process for LSAW pipes," *J Mater Process Technol*, vol. 255, pp. 150–160, May 2018, doi: 10.1016/j.jmatprotec.2017.11.060.

[17] Z. Zhang, J. Wu, X. Xu, Z. Yang, W. Wu, and L. Liu, "Mechanical Modeling of Tube Bending Considering Elastoplastic Evolution of Tube Cross- Section," *Materials*, vol. 15, no. 11, Jun. 2022, doi: 10.3390/ma15113997.

[18] S. Iswahyudi, "Kajian Teoretis Kerutan di Daerah Tekukan pada Pipa Hasil Proses Bending," *Jurnal Teknik Mesin*, vol. 14, no. 1, Sep. 2013, doi: 10.9744/jtm.14.1.47-51.

[19] S. F. Lajarin, R. A. C. Filho, C. J. Rebeyka, C. P. Nikhare, and P. V. P. Marcondes, "Numerical study on variation of chord modulus on the springback of high-strength steels," *International Journal of Advanced Manufacturing Technology*, vol. 106, no. 11–12, pp. 4707–4713, Feb. 2020, doi: 10.1007/s00170-020-04975-x.

[20] A. Mohammed and K. A. Cashell, "Structural fire design of SHS, RHS and CHS high strength steel columns," *Advances in Structural Engineering*, vol. 24, no. 11, pp. 2390–2401, Aug. 2021, doi: 10.1177/13694332211001498.

[21] Y. Wu, Z. Wang, J. Tian, R. Chen, W. Lin, and Y. Lin, "Study on the thinning characteristics of aviation tubes during bending forming under boundary lubrication friction," *J Manuf Process*, vol. 149, pp. 443–455, Sep. 2025, doi: 10.1016/j.jmapro.2025.05.081.